Kinetically-Driven Phase Transformation during Lithiation in Copper Sulfide Nanoflakes

Kai He,*[†,‡] Zhenpeng Yao,[†] Sooyeon Hwang,[‡] Na Li,[§] Ke Sun,[∥] Hong Gan,[∥] Yaping Du,[§] Hua Zhang,[⊥] Chris Wolverton,[†] and Dong Su*[‡]

[†]Department of Materials Science and Engineering, Northwestern University, Evanston, Illinois 60208, United States

[‡]Center for Functional Nanomaterials, Brookhaven National Laboratory, Upton, New York 11953, United States

[§]Frontier Institute of Science and Technology jointly with College of Science, State Key Laboratory for Mechanical Behavior of Materials, Xi'an Jiaotong University, Xi'an 710054, China

[∥]Energy Sciences Directorate, Brookhaven National Laboratory, Upton, New York 11953, United States

[⊥]Center for Programmable Materials, School of Materials Science and Engineering, Nanyang Technological University, Singapore 639798, Singapore

S *Supporting Information*

ABSTRACT: Two-dimensional (2D) transition metal chalcogenides have been widely studied and utilized as electrode materials for lithium ion batteries due to their unique layered structures to accommodate reversible lithium insertion. Real-time observation and mechanistic understanding of the phase transformations during lithiation of these materials are critically important for improving battery performance by controlling structures and reaction pathways. Here, we use in situ transmission electron microscopy methods to study the structural, morphological, and chemical evolutions in individ-

ual copper sulfide (CuS) nanoflakes during lithiation. We report a highly kinetically driven phase transformation in which lithium ions rapidly intercalate into the 2D van der Waals-stacked interlayers in the initial stage, and further lithiation induces the Cu extrusion via a displacement reaction mechanism that is different from the typical conversion reactions. Density functional theory calculations have confirmed both the thermodynamically favored and the kinetically driven reaction pathways. Our findings elucidate the reaction pathways of the Li/CuS system under nonequilibrium conditions and provide valuable insight into the atomistic lithiation mechanisms of transition metal sulfides in general.

KEYWORDS: Copper sulfides, CuS, electrochemistry kinetics, lithium ion battery, in situ TEM
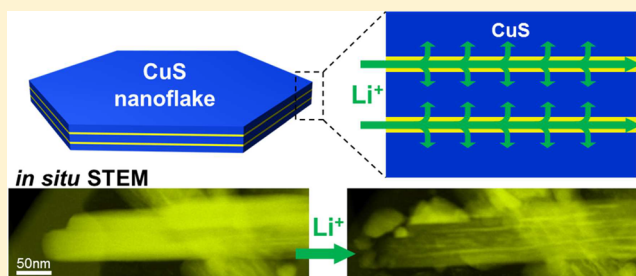
Lithium ion batteries (LIBs) are currently the dominant technology to fulfill the energy storage demand in portable electronic devices and electric vehicles and could play a key role in linking intermittent renewable energy sources to practical use on the grid scale.[1−3] As the key component of LIBs, the electrode materials primarily determine the battery's energy and power density, that is, the specific capacity and rate capability, and thus are the main focus of much current research. Traditional cathode materials, such as layered transition metal oxides (e.g., $LiCoO_2$) and phosphide-olivines (e.g., $LiFePO_4$), have ordered open channels to allow lithium ions reversibly intercalate into and out of the host structures without collapse of the close-packed oxygen frameworks.[4−7] Conversion electrodes can achieve a higher lithium storage capacity by solid-state conversion reactions with compounds that do not have accompanying interstitial space, resulting in a complete structural rearrangement with dramatic volume change, and thus poor cyclability.[7−9] Recent development of two-dimensional (2D) transition metal chalcogenides provides new choices for battery electrodes since they have intercalation

channels to enhance the reaction cyclability and proceed via a conversion reaction to maintain their high capacities.[10−12] As a member of this family, copper sulfide (CuS) exhibits a similar 2D layered structure as many others in which the layers composed of Cu−S tetrahedrons are separated by van der Waals S−S bonds, providing open channels to facilitate fast lithium intercalation. This phenomenon has been observed in similar metal sulfides such as TiS_2, MoS_2, and SnS_2.[13−18] Benefited from the recent advancement of in situ transmission electron microscopy (TEM) with higher spatial resolution,[19−24] McDowell et al. reported the observation of real-time phase transformations in multiple metal sulfides (Cu_2S, Fe_2S, and Co_3S_4) on the atomic scale,[22] but the detailed evolution of such dynamic processes in CuS still remains elusive.
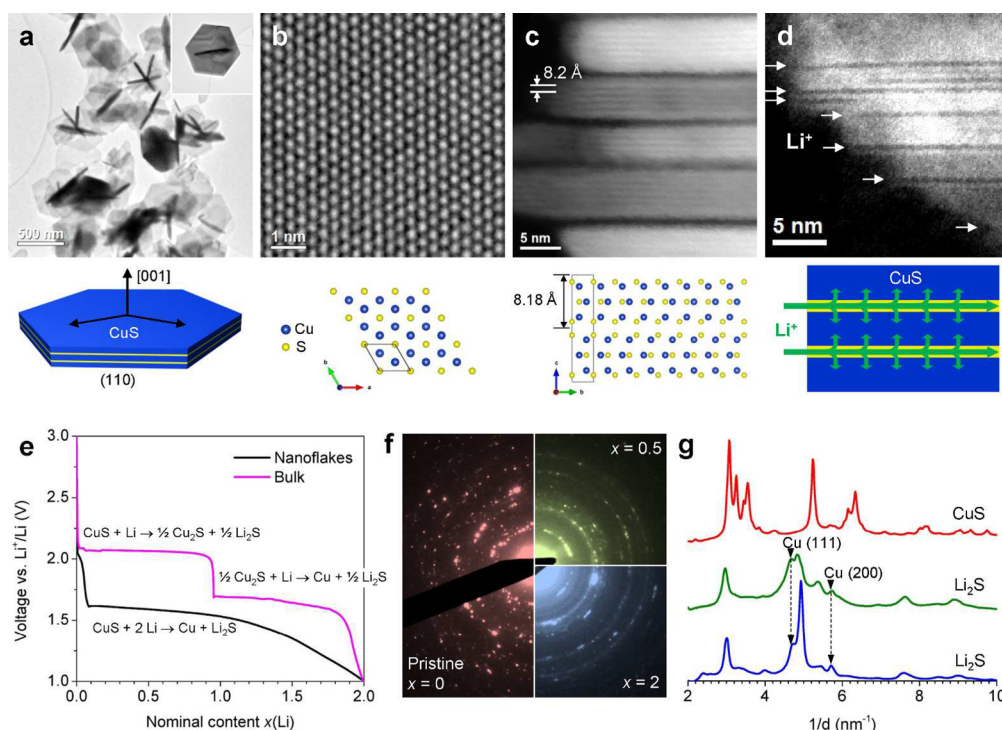
**Figure 1.** (a) TEM image of as-synthesized CuS nanoflakes with hexagonal geometry shown in the inset and schematic illustration shown below. High-resolution TEM (b) and ADF-STEM (c) images showing plan-view and cross-sectional crystal structures along [001] and [100] directions with corresponding atomic models listed below. (d) ADF-STEM image of partially lithiated CuS (lithium content $x = 0.5$) showing lithium intercalating into interlayer spaces (indicated by white arrows) with a schematic illustration shown below. (e) The first-cycle discharge curves of CuS nanoflakes and bulk materials. (f) Electron diffraction patterns of lithiated electrode with lithium content $x = 0, 0.5, 2$, respectively. (g) The radially averaged intensity profiles corresponding to the diffraction patterns in (f), in which Cu(111) and (200) peaks are labeled by dashed arrow lines, and other peaks correspond to either CuS or Li_2S as labeled. Detailed analysis procedures can be found in Figure S1.

Previous studies have revealed that the full lithiation of CuS follows the equation similar to a conversion reaction to allow for 2 Li^+ ions being stored for each CuS formula unit[25−33]

$$CuS + 2Li^+ + 2e^- \rightarrow Cu + Li_2S \qquad (1)$$
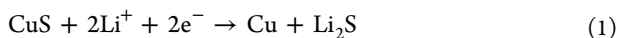
Under conditions of thermodynamic equilibrium, this reaction would proceed through a two-step process to produce Cu_2S and Cu sequentially as revealed by X-ray diffraction[25−28]

$$CuS + Li^+ + e^- \rightarrow 0.5Cu_2S + 0.5Li_2S \qquad (2)$$

$$0.5Cu_2S + Li^+ + e^- \rightarrow Cu + 0.5Li_2S \qquad (3)$$
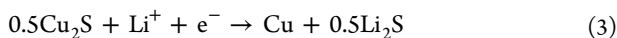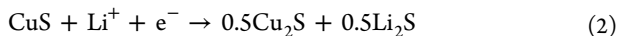
where Cu is reduced from 2+ to 1+ in the eq 2, when lithium ions break the interlayer van der Waals S−S bonds but keep the overall anion framework intact, and further lead to the extrusion of Cu metal and microscopic phase separation (so-called displacement reaction)[26,27] in eq 3. However, in practical cases where nonequilibrium conditions such as local concentration of lithium, local stress and electrochemical overpotential are generally applied, there have been a diversity of proposed reaction paths, such as disproportionation reaction and conversion reaction (nanoscopic phase separation associated with dispersive metal nanoprecipitation and complete destruction of host structures).[25,26,29−32] Although recent development showed improved cycling performance of CuS by nanostructuring, where kinetic effects tend to be more pronounced due to the dramatic size reduction and usually play a key role in the determination of the reaction paths, it is still unclear whether the lithiation of copper sulfide dictates a displacement or conversion mechanism, the answer to which may provide

implications for a general group of metal sulfide materials as LIB electrodes. It is also noted that precise identification of intermediate phases during phase transformation of CuS appears to be difficult due to the existence of many nonstoichiometric copper sulfides, such as djurleite ($Cu_{1.96}S$), digenite ($Cu_{1.8}S$), and anilite ($Cu_{1.75}S$) in addition to the most stable covellite (CuS) and chalcocite (Cu_2S) phases, especially when the samples were examined by post-mortem X-ray or electron microscopy techniques at conditions far away from the operando state.[25,26] Density functional theory (DFT) calculations have been widely used as compelling tools for battery research to discover new electrode materials, explore the electrochemical reaction kinetics, and particularly, predict equilibrium and nonequilibrium phase transformations during charge and discharge.[34−40] Therefore, in situ TEM with the help of first-principles calculations would offer an intriguing chance to accurately reveal the detailed underlying mechanisms at the atomistic scale, which is often difficult to obtain solely via conventional experiments.

Here, we use in situ scanning transmission electron microscopy (STEM) techniques to track the structural and chemical evolution and phase transformations during lithiation in individual single-crystal CuS nanoflakes. DFT calculations elucidate the detailed structural evolution, which is consistent with in situ and analytical TEM observations. The proposed reaction mechanism can interpret the overall electrochemical discharge profile that represents the collective behavior of the entire nanocrystals. These findings uncover the reaction pathways of the Li/CuS system and shed light on the mechanistic understanding of phase transformations in general
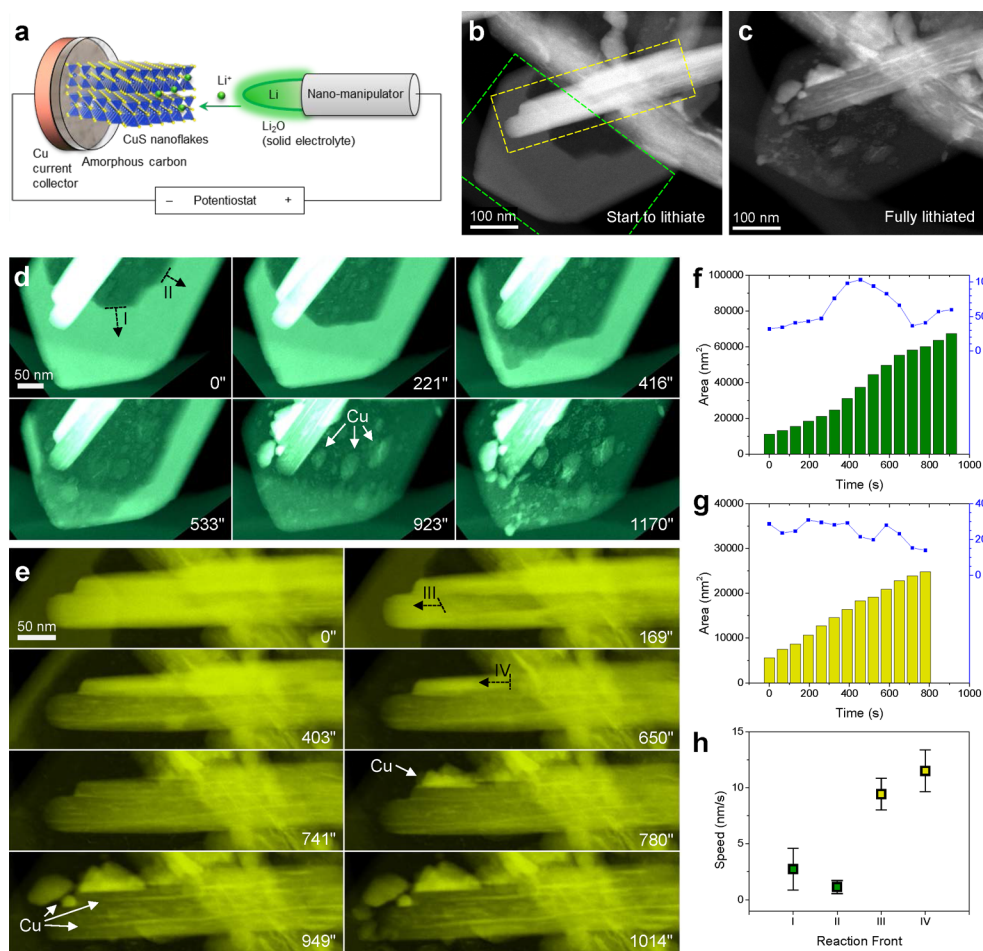
Figure 2. (a) Schematics showing in situ battery setup for S/TEM observation. STEM images of CuS nanoflakes before (b) and after (c) lithiation. Time sequential STEM images during in situ lithiation showing reaction in plan-view (d) and side-view (e), corresponding to the areas of green and yellow dashed boxes in (b), respectively. Reacted area and areal speed (time derivative) as a function of time of plan-view (f) and side-view (g) lithiation. Details also shown in Figure S2. (h) Averaged propagation speed of four representative reaction fronts (I, II, III and IV, marked by dashed arrows).

metal sulfides materials with fast lithiation channels induced by van der Waals interlayers.

We use CuS nanoflakes synthesized via a soft-template approach as the active electrode material for LIBs,[33] because they exhibit the well-defined geometry with hexagonal basal plane ~200 nm and thickness 5−20 nm, as shown in Figure 1a. The HRTEM and HR-STEM images in Figure 1b,c show the atomic arrangement along the plan-view ([001] direction) and side-view ([100] direction), respectively, which indicate the layered structure separated by S—S van der Waals bonds every half unit cell (~8.2 Å). Such nanoscale ultrathin flake geometry provides an ideal platform for investigating their electrochemical reactions versus lithium and understanding the underlying atomistic mechanism. By examining the electrode material after a partial discharge reaction, we found the planar lithiation channels appearing as the dark lines propagating from surface to inner region in the side-view annular dark-field (ADF) STEM image (Figure 1d), which is consistent with the lithiation pathway previously reported in 2D metal sulfides.[17,18] It is also noted that some channels are not open to the sample surface, implying that those channels would be activated by cross-linking lithium diffusion across the interlayer spacing, but this phenomenon was not observed by in situ experiments shown below. We also assembled coin-cell batteries and

measured the electrochemical properties for CuS nanoflakes and the counterpart in the bulk form. Figure 1e shows the first-cycle discharge curves of both nano- and bulk-CuS materials, in which the bulk CuS displays two well-defined discharge plateaus corresponding to the two-step reactions shown in eqs 2 and 3, whereas the CuS nanoflakes show a single declining plateau corresponding to the overall reaction in eq 1. By analyzing the globally averaged electron diffraction patterns (Figure 1f) obtained at different states of discharge (x = 0, 0.5, 2), we found that the pristine CuS nanocrystals gradually transformed into the mixed Cu and Li_2S phases, and the intensity of Cu peaks became more pronounced as lithiation proceeded, as indicated in Figure 1g. The fact that we do not observe the Cu_2S intermediate phase, contrary to the bulk electrode, is similar to our previous observation on spinel iron oxides and is likely attributed to kinetic, nonequilibrium effects that must be taken into account as the Li diffusion length of active materials has been dramatically reduced to the nanoscale.[41,42] Therefore, elucidating these kinetically driven phase transformations depends critically on the real-time characterization using in situ techniques.

We use the dry-format electrochemical cell setup for in situ S/TEM observations, as illustrated in Figure 2a, in which CuS nanoflakes on amorphous carbon support and Li metal play as

the two electrodes and native Li_2O coating formed on Li tip serves as solid-state electrolyte (details described in Methods).[41−43] Because the CuS nanoflakes are attached to each other in random orientations after drop casting onto the amorphous carbon support, this allows for simultaneous observation from both plan-view and side-view. Figure 2b,c shows the samples of interest (green dashed box for plan-view and yellow dashed box for side-view) before and after lithiation observed by ADF-STEM (also see Supporting Information Movie S1). The cropped time-lapse STEM image series are shown in Figure 2d,e, respectively. As seen in Figure 2d, the lithiation of the planar nanoflake has started at the beginning of the in situ movies, resulting in the darker contrast in the lithiated region than the pristine region with sharp reaction fronts in between. This process (contrast change from bright to dark) represents the intercalation of Li ions into the CuS interlayers. As lithiation further proceeds, the reaction fronts move toward the edges of hexagon until the entire nanoflake is intercalated with lithium (923 s). In the meantime, a number of Cu nanoparticles (NPs) precipitate on the surface of reacted region (indicated by white arrows), and they agglomerate rapidly to form larger particles with size >50 nm, which is distinct from the typical conversion reaction that forms ultrafine (<5 nm) and highly dispersive NPs in the host matrix.[22,41−44] This process corresponds to the displacement reaction associated with extrusion of metallic Cu NPs by inserting excess Li ions.[22,26] It is worth noting that the processes of Li intercalation and Cu extrusion are largely overlapping in the time scale of the experiment, which tend to merge the nominal two reactions at different electrochemical potentials into one voltage plateau (Figure 1e).[41,44] The lithiation of another CuS nanoflake observed from the side-view (Figure 2e) similarly exhibits two processes of Li intercalation (0−741 s) and Cu extrusion (780−1014 s), respectively, but it is clearly revealed that in addition to precipitation on free surfaces, Cu extrusion can also occur within the interlayer channels (indicated by white arrows at 949 s) and consequently pop out Cu NPs on the edge of nanoflake. It is also noted that the Li intercalation and Cu extrusion in this scenario happen in a sequential order without any overlap. The diversity of reaction modality can be universally found in reproducible experiments (another representative example shown in Movie S3) due to different kinetic effects induced by the localized electrochemical environments. By comparing the reaction area change versus time in both viewing directions (Figure 2f,g), we found that the lithiation behaviors in two nanoflakes are similar and comparable. However, the propagation speeds of Li intercalation reaction fronts are quite different; the speed of side-view lithiation (III and IV, marked by black dash arrows) is faster than that of plan-view lithiation (I and II), as shown in Figure 2h. This explains why Li intercalation finishes before the start of Cu extrusion in the side-view case and implies that the competition of two processes is determined by the local kinetics factors.

Figure 3 shows the analytical characterization of elemental distribution in a lithiated sample by electron energy-loss spectroscopy (EELS) technique. The overall EELS spectrum of the lithiated sample (Figure 3c) displays the characteristic low-loss energy edges of Li (K-edge, 55 eV), Cu ($M_{2,3}$ edges, 74 eV), and S ($L_{2,3}$ edges, 165 eV) elements. From the STEM-EELS mapping (Figure 3b), it is obvious that two phases, copper and lithium sulfide, exist after lithiation, corresponding to the bright and dark regions in Figure 3a, respectively.
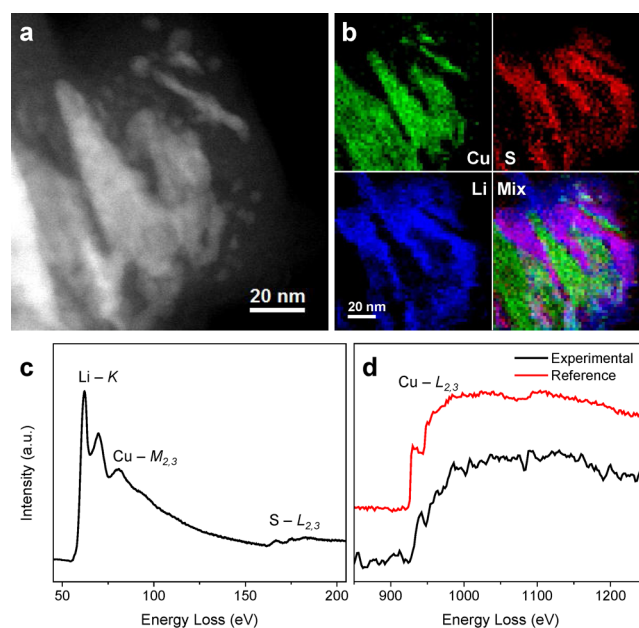
Figure 3. (a) STEM image of CuS nanoflakes after a complete lithiation. (b) The corresponding STEM-EELS maps showing Cu (green), S (red), and Li (blue) distributions; the purple areas in the overlaid mix map correspond to Li_2S. (c) EELS spectrum showing low-loss characteristic energy edges (Li-K, Cu-$M_{2,3}$, S-$L_{2,3}$) in the lithiated sample. (d) Experimental (black) and standard (red, from pure Cu metal in Gatan EELS Atlas) EELS spectra of the core-loss Cu-$L_{2,3}$ edges indicating the Cu in metallic state after lithiation.

Because the pristine CuS sample contains copper in oxidation state (Cu^{2+}, shown in Figure S4), to avoid any misinterpretation we also acquired core-less EELS spectrum from the precipitates (Figure 3d) from which the fine structures of Cu $L_{2,3}$ edges exclusively identify the extrusion to be metallic Cu. Interestingly, we also found that the extruded Cu NPs would not stay dispersed in the Li_2S matrix but rather tend to hop around the surface and gather into large domains (see Supporting Information Movie S2 and Figures S4 and S5). This demonstrates the high mobility of Cu,[22,26] which also implies that the extruded Cu could quickly migrate back into the host structure in the reverse reaction (delithiation), though such a process may not be completely reversible, as shown in Movie S4.

We investigated the lithiation process of CuS using DFT calculations by exploring both equilibrium and nonequilibrium reaction pathways using approaches as described in Methods. To simulate the equilibrium path, the ternary Li−Cu−S phase diagram (0 K) was constructed by calculating formation energies of all known compounds of the Li−Cu−S chemical space with structures adopted from the Inorganic Crystal Structure Database (ICSD).[45,46] The ground state Li-CuS reaction was found to go through two three-phase regions (Figure S6). A two-step lithiation route is therefore suggested (CuS + Li → Cu_2S + Li_2S → Cu + Li_2S) as observed in bulk CuS systems. The corresponding equilibrium lithiation voltage profile was calculated which shows a similar trend with the experimental discharge voltage curve of the bulk CuS materials (Figure S7). It is noteworthy that the discharge curve measured from the nanoflakes exhibits large differences from the one measured in bulk materials and voltage profile predicted by the equilibrium lithiation (Figure 1e and Figure S7), suggesting an alternative reaction path for the lithiation processes of the CuS
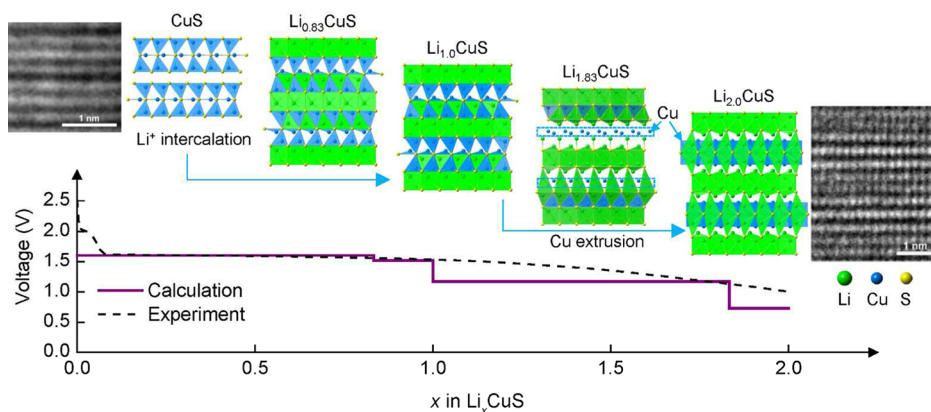
Figure 4. DFT calculated discharge voltage profile and atomic models corresponding to the predicted intermediate phases during the nonequilibrium lithiation process in CuS nanocrystals. The black dashed line indicates experimental discharge curve. Two HRTEM images show good structural agreement for both pristine CuS (left) and final Li_2CuS (right).

nanoflakes. As a result, we focused on the nonequilibrium lithiation pathways involving intermediate structures as the source of the shape and magnitude variations from the equilibrium voltages. We studied the nonequilibrium lithiation process of CuS by the prediction of nonequilibrium structures along the discharge pathway based on geometrical enumeration and total energy screening (see Methods). We were able to identify a series of nonequilibrium phases constituting a metastable Li−CuS convex hull as shown in Figure S8. The calculated nonequilibrium voltage profile shows reasonable agreement with the experimental discharge curve for the lithiation of CuS nanoflakes (Figure 4 and Figure S7). We then looked into the atomistic structural evolution during the nonequilibrium lithiation. As displayed in the upper panel of Figure 4, during the nonequilibrium lithiation Li ions would first intercalate into the interlayer channels held by van der Waals bonds, and then fill up the open tetrahedral sites on both sides of the interlayer spacing, forming $Li_{1.0}CuS$ with Cu^{2+} partially reduced to Cu^{1+} (Figure S9a). Afterward, further Li insertion (up to 6 per unit cell) would take the remaining empty tetrahedral sites and gradually extrude the fully reduced Cu^0 atoms, resulting in a nominal composition of $Li_{2.0}CuS$, followed by the phase separation into Cu and Li_2S. The final phase is characterized by alternative Cu and Li layers. The evolution of atomic structure confirms the lithiation through the displacement mechanism and matches with HRTEM observations at the pristine and final states.

In summary, using ultrathin hexagonal CuS nanoflakes as a model material, we have investigated the phase transformations in the CuS/Li electrochemical system. The dynamical morphological and structural evolution during lithiation was observed in both plan-view and side-view using in situ ADF-STEM, which explicitly revealed the two-step lithiation pathway through Li intercalation and Cu extrusion, respectively, which can be overlapped or in the sequential order depending on the localized kinetic effect. We clarified that the Cu extrusion from CuS nanoflakes proceeded through the displacement mechanism rather than direct conversion reaction. The 2D interlayer channels held by van der Waals bonds provide a fast Li intercalation path and facilitate further Li and Cu migration as well. Combining in situ S/TEM observation with DFT calculation, the atomistic mechanism of nonequilibrium lithiation in CuS nanoflakes has been uncovered, which is suggested to be responsible for the flattened voltage profile in

the first discharge under realistic kinetic circumstances. Our findings obtained from CuS nanoflakes shed light on the mechanistic understanding of nanoscale lithiation in other 2D transition metal chalcogenide systems.

■ METHODS

Materials Synthesis. The CuS nanoflakes were synthesized using a soft-template method.[33] CuCl (1.5 mmol) was added to the mixture of 5 mL oleylamine (OM) and 5 mL octylamine (OTA) in a three-necked flask (100 mL) at room temperature, then the slurry was heated to 100 °C to remove water and oxygen with vigorous magnetic stirring under vacuum for ~30 min in a temperature-controlled electromantle. The solution was maintained at 130 °C for 4 h and became transparent. Then, the S dispersion formed by ultrasonication of 4.5 mmol of S powder in the mixture of 2.5 mL OTA and 2.5 mL OM at room temperature was quickly injected into the resulting solution at 95 °C. After the resulting mixture was kept at 95 °C for 18 h, it became dark. After cooling down to room temperature, the CuS nanoflakes were precipitated by adding excess absolute ethanol (~40 mL) to the solution and then collected by centrifugation at 8500 r.p.m. for 20 min.

TEM Characterization. The in situ TEM electrochemical cell was incorporated into a Nanofactory TEM-STM specimen holder (Figure 2a),[41−44] in which CuS nanoflakes dispersed on a TEM half-grid with amorphous carbon support are analogous to active electrode material, current collector, and carbon binders, respectively; Li metal was coated on to a piezo-driven W probe as the counter electrode with a thin layer of Li_2O formed on Li metal as the solid electrolyte. The Li and CuS were loaded on to the holder in an Ar-filled glovebox and then transferred to the TEM column using a sealed Ar bag to avoid exposing them to air. A constant dc potential up to ±2.5 V was applied to CuS electrode against the Li source during in situ (de)lithiation, and the (de)lithiation processes were captured in real-time in either the TEM or STEM mode on a JEOL 2100F TEM operated at 200 kV. Analytical TEM was partially performed on a Hitachi HD2700C STEM with a probe aberration corrector. Electron diffraction patterns were acquired at different states of charge and the radially averaged intensity profiles can be obtained by rotational integration around the direct beam (Figure S1). The analysis of reaction area was based on the contrast difference in STEM images and details of

outlining boundaries between reacted and pristine phases can be found in Figure S2.

Electrochemical Measurement. The electrodes were prepared by mixing CuS active materials with carbon black (TIMCAL) and PVDF (Alfa Aesar) in 1-methyl-2-pyrrolidone (Alfa Aesar) into a homogeneous slurry, which was cast onto an aluminum foil using a doctor blade. The electrodes were dried in a fume hood under continuous dry air flow (dew point lower than −40 °C) for 24 h before transferring into an oven heated at 50 °C for another 24 h to eliminate residue solvent and moisture. The 2032 coin cells were assembled by using electrodes prepared above as working electrode and a lithium disk as both counter and reference electrode with Celgard (2325) separator in between to prevent shorting. The electrolyte was lithium hexafluorophosphate $(LiPF_6)$ (1 M) in ethylene carbonate/dimethyl carbonate (EC/DMC) (volume ratio 50:50). The electrochemical measurements were conducted at room temperature using a Biologic (VMP3) battery cycler. The cells were cycled galvanostatically at 0.1C (56 mAh g^{-1}) between 1.0 and 3.0 V.

First-Principles Calculations. First-principles density functional theory (DFT) calculations were performed via the Vienna Ab-initio Simulation Package (VASP)[47−49] with the projector augmented wave (PAW) potentials.[50] For the exchange-correlation functional, generalized gradient approximation (GGA) of Perdew−Becke−Ernzerhof (PBE)[51] was used with spin polarization and the vdW-D2 functional was adopted including a self-consistent van der Waals (vdW) correction.[52,53] Two different sets of parameters were used with one for lower energy configuration sampling, and the other for accurate total energy determination. For coarse sampling calculations, we used kinetic energy cutoffs of 300 eV for the plane wave basis set, and Γ-centered grids of approximately 4000 k-points per reciprocal atom. The accurate calculations were conducted with a plane-wave basis set cutoff energy of 520 eV, and Γ-centered k-meshes with the density of 8000 k-points per reciprocal atom were used in related calculations.

To search for the nonequilibrium phases through the Li-CuS reaction, the Non-Equilibrium Phase Search (NEPS) method[54,55] was applied by exploring geometrically distinct Li/vacancy configurations on possible insertion sites of CuS structure at different compositions (Li/vacancy ratios). We assumed that Li diffusion in transition metal sulfides is significantly faster than transition metal and sulfur ions during the lithiation reaction following previous studies.[56,57] Li ion(s) therefore can take any energetically favored unoccupied site(s) while the migrations of transition metal and sulfur ions are limited, enabling the nonequilibrium lithiation process. The method proceeds as follows (Figure S10): (i) Identify all possible insertion sites in the original CuS structure using MINT.[58−60] CuS adopts a hexagonal covellite structure with unoccupied inlayer (A) and interlayer (B) as shown in Figure S10a. A supercell containing 6 Cu^{2+} and S^{2-} ions was built which has 12 total empty sites that Li ions can insert. (ii) Generate all symmetrically distinct configurations with Enum[61−63] for a series of compositions $Li_x\square_{2-x}CuS$ (0 < x < 2, $\square$ denoting vacancy). (iii) Sample total energies of all configurations with settings described in the previous section. (iv) For the specific composition, corresponding structures were ranked by their total energies and the three lowest energy structures were further relaxed in DFT with more strict settings. Formation energies of selected structures were then calculated according to following reaction: $CuS + xLi \rightarrow Li_xCuS$. (v) Build

the lithiation convex hull using the formation energies and the composition points on the hull were determined to be the nonequilibrium intermediate phases.

The details of the construction of the Li−Cu−S phase diagram and equilibrium reaction path, as well as the calculation of voltage profiles are described in Supporting Information.

■ ASSOCIATED CONTENT

ⓢ Supporting Information

The Supporting Information is available free of charge on the ACS Publications website at DOI: 10.1021/acs.nano-lett.7b02694.

> (Additional details of S/TEM images, electron diffraction, EELS, DFT calculation PDF)
>
> In situ STEM observation showing lithiation of CuS nanoflakes along both plan-view and side-view. The movie clip is accelerated by 100 times (AVI)
>
> In situ TEM observation showing Cu extrusion and hopping during lithiation of CuS nanoflakes. The movie clip is accelerated by 50 times (AVI)
>
> In situ STEM observation showing another representative lithiation of CuS nanoflakes. The movie clip is accelerated by 100 times (AVI)
>
> In situ STEM observation showing delithiation of the CuS nanoflakes after the lithiation in Movie S3. The movie clip is accelerated by 150 times (AVI)

■ AUTHOR INFORMATION

Corresponding Authors
*E-mail: he@northwestern.edu.
*E-mail: dsu@bnl.gov.

ORCID ⓘ
Kai He: 0000-0003-4666-1800
Yaping Du: 0000-0002-9937-2087
Hua Zhang: 0000-0001-9518-740X
Chris Wolverton: 0000-0003-2248-474X
Dong Su: 0000-0002-1921-6683

Author Contributions
K.H. and D.S. conceived and designed the experiments. K.H., S.H., and D.S. performed the in situ and ex situ S/TEM experiments. Z.Y. and C.W. performed the theoretical calculation. Y.D., N.L., and H.Z. synthesized the CuS nanoflakes. K.S. and H.G. performed the electrochemical measurements. K.H. and D.S. wrote the manuscript. All authors participated in discussions of the results.

Notes
The authors declare no competing financial interest.

■ ACKNOWLEDGMENTS

■ REFERENCES

(1) Armand, M.; Tarascon, J. M. *Nature* **2008**, *451*, 652−657.

(2) Dunn, B.; Kamath, H.; Tarascon, J. M. *Science* **2011**, *334*, 928−935.

(3) Larcher, D.; Tarascon, J. M. *Nat. Chem.* **2014**, *7*, 19−29.

(4) Bruce, P. G.; Scrosati, B.; Tarascon, J. M. *Angew. Chem., Int. Ed.* **2008**, *47*, 2930−2946.

(5) Whittingham, M. S. *Chem. Rev.* **2004**, *104*, 4271−4301.

(6) Kang, K.; Meng, Y. S.; Breger, J.; Grey, C. P.; Ceder, G. *Science* **2006**, *311*, 977−980.

(7) Nitta, N.; Wu, F.; Lee, J. T.; Yushin, G. *Mater. Today* **2015**, *18*, 252−264.

(8) Poizot, P.; Laruelle, S.; Grugeon, S.; Dupont, L.; Tarascon, J. M. *Nature* **2000**, *407*, 496−499.

(9) Cabana, J.; Monconduit, L.; Larcher, D.; Palacin, M. R. *Adv. Mater.* **2010**, *22*, E170−E192.

(10) Chhowalla, M.; Shin, H. S.; Eda, G.; Li, L. J.; Loh, K. P.; Zhang, H. *Nat. Chem.* **2013**, *5*, 263−275.

(11) Gao, M. R.; Xu, Y. F.; Jiang, J.; Yu, S. H. *Chem. Soc. Rev.* **2013**, *42*, 2986−3017.

(12) Stephenson, T.; Li, Z.; Olsen, B.; Mitlin, D. *Energy Environ. Sci.* **2014**, *7*, 209−231.

(13) Julien, C. M. *Mater. Sci. Eng., R* **2003**, *40*, 47−102.

(14) Hu, X.; Zhang, W.; Liu, X.; Mei, Y.; Huang, Y. *Chem. Soc. Rev.* **2015**, *44*, 2376−2404.

(15) Wan, J.; Bao, W.; Liu, Y.; Dai, J.; Shen, F.; Zhou, L.; Cai, X.; Urban, D.; Li, Y.; Jungjohann, K.; Fuhrer, M. S.; Hu, L. *Adv. Energy Mater.* **2015**, *5*, 1401742.

(16) Zeng, Z.; Zhang, X.; Bustillo, K.; Niu, K.; Gammer, C.; Xu, J.; Zheng, H. *Nano Lett.* **2015**, *15*, 5214−5220.

(17) Kushima, A.; Qian, X.; Zhao, P.; Zhang, S.; Li, J. *Nano Lett.* **2015**, *15*, 1302−1308.

(18) Gao, P.; Wang, L.; Zhang, Y. Y.; Huang, Y.; Liao, L.; Sutter, P.; Liu, K.; Yu, D.; Wang, E. G. *Nano Lett.* **2016**, *16*, 5582−5588.

(19) Liu, X. H.; Wang, J. W.; Huang, S.; Fan, F.; Huang, X.; Liu, Y.; Krylyuk, S.; Yoo, J.; Dayeh, S. A.; Davydov, A. V.; Mao, S. X.; Picraux, S. T.; Zhang, S.; Li, J.; Zhu, T.; Huang, J. Y. *Nat. Nanotechnol.* **2012**, *7*, 749−756.

(20) Nie, A.; Gan, L. Y.; Cheng, Y.; Asayesh-Ardakani, H.; Li, Q.; Dong, C.; Tao, R.; Mashayek, F.; Wang, H. T.; Schwingenschlogl, U.; Klie, R. F.; Yassar, R. S. *ACS Nano* **2013**, *7*, 6203−6211.

(21) Gu, M.; Kushima, A.; Shao, Y.; Zhang, J. G.; Liu, J.; Browning, N. D.; Li, J.; Wang, C. *Nano Lett.* **2013**, *13*, 5203−5211.

(22) McDowell, M. T.; Lu, Z.; Koski, K. J.; Yu, J. H.; Zheng, G.; Cui, Y. *Nano Lett.* **2015**, *15*, 1264−1271.

(23) Liu, Y.; Fan, F.; Wang, J. W.; Liu, Y.; Chen, H. L.; Jungjohann, K. L.; Xu, Y.; Zhu, Y.; Bigio, D.; Zhu, T.; Wang, C. S. *Nano Lett.* **2014**, *14*, 3445−3452.

(24) Gong, Y.; Zhang, J.; Jiang, L.; Shi, J. A.; Zhang, Q.; Yang, Z.; Zou, D.; Wang, J.; Yu, X.; Xiao, R.; Hu, Y. S.; Gu, L.; Li, H.; Chen, L. *J. Am. Chem. Soc.* **2017**, *139*, 4274−4277.

(25) Chung, J. S.; Sohn, H. J. *J. Power Sources* **2002**, *108*, 226−231.

(26) Debart, A.; Dupont, L.; Patrice, R.; Tarascon, J. M. *Solid State Sci.* **2006**, *8*, 640−651.

(27) Jache, B.; Mogwitz, B.; Klein, F.; Adelhelm, P. *J. Power Sources* **2014**, *247*, 703−711.

(28) Li, X.; He, X.; Shi, C.; Liu, B.; Zhang, Y.; Wu, S.; Zhu, Z.; Zhao, J. *ChemSusChem* **2014**, *7*, 3328−3333.

(29) Wang, Y.; Zhang, X.; Chen, P.; Liao, H.; Cheng, S. *Electrochim. Acta* **2012**, *80*, 264−268.

(30) Sun, K.; Su, D.; Zhang, Q.; Bock, D. C.; Marschilok, A. C.; Takeuchi, K. J.; Takeuchi, E. S.; Gan, H. *J. Electrochem. Soc.* **2015**, *162*, A2834−A2839.

(31) Chen, Y.; Davoisne, C.; Tarascon, J. M.; Guéry, C. *J. Mater. Chem.* **2012**, *22*, 5295−5299.

(32) Ren, Y.; Wei, H.; Yang, B.; Wang, J.; Ding, J. *Electrochim. Acta* **2014**, *145*, 193−200.

(33) Du, Y.; Yin, Z.; Zhu, J.; Huang, X.; Wu, X. J.; Zeng, Z.; Yan, Q.; Zhang, H. *Nat. Commun.* **2012**, *3*, 1177.

(34) Thackeray, M. M.; Wolverton, C.; Isaacs, E. D. *Energy Environ. Sci.* **2012**, *5*, 7854−7863.

(35) Li, Q.; Liu, H.; Yao, Z.; Cheng, J.; Li, T.; Li, Y.; Wolverton, C.; Wu, J.; Dravid, V. P. *ACS Nano* **2016**, *10*, 8788−8795.

(36) Wolverton, C.; Zunger, A. *Phys. Rev. Lett.* **1998**, *81*, 606−609.

(37) Ceder, G.; Chiang, Y.-M.; Sadoway, D. R.; Aydinol, M. K.; Jang, Y.-I.; Huang, B. *Nature* **1998**, *392*, 694−696.

(38) Morgan, D.; Van der Ven, A.; Ceder, G. *Electrochem. Solid-State Lett.* **2004**, *7*, A30−A32.

(39) Meng, Y. S.; Arroyo-de Dompablo, M. E. *Energy Environ. Sci.* **2009**, *2*, 589−609.

(40) Bin, H.; Yao, Z.; Zhu, S.; Zhu, C.; Pan, H.; Chen, Z.; Wolverton, C.; Zhang, D. *J. Alloys Compd.* **2017**, *695*, 1223−1230.

(41) He, K.; Zhang, S.; Li, J.; Yu, X.; Meng, Q.; Zhu, Y.; Hu, E.; Sun, K.; Yun, H.; Yang, X. Q.; Zhu, Y.; Gan, H.; Mo, Y.; Stach, E. A.; Murray, C. B.; Su, D. *Nat. Commun.* **2016**, *7*, 11441.

(42) He, K.; Lin, F.; Zhu, Y.; Yu, X.; Li, J.; Lin, R.; Nordlund, D.; Weng, T. C.; Richards, R. M.; Yang, X. Q.; Doeff, M.; Stach, E. A.; Mo, Y.; Xin, H. L.; Su, D. *Nano Lett.* **2015**, *15*, 5755−5763.

(43) He, K.; Xin, H. L.; Zhao, K.; Yu, X.; Nordlund, D.; Weng, T. C.; Li, J.; Jiang, Y.; Cadigan, C. A.; Richards, R. M.; Doeff, M. M.; Yang, X. Q.; Stach, E. A.; Li, J.; Lin, F.; Su, D. *Nano Lett.* **2015**, *15*, 1437−1444.

(44) Li, J.; He, K.; Meng, Q.; Li, X.; Zhu, Y.; Hwang, S.; Sun, K.; Gan, H.; Zhu, Y.; Mo, Y.; Stach, E. A.; Su, D. *ACS Nano* **2016**, *10*, 9577−9585.

(45) Belsky, A.; Hellenbrandt, M.; Karen, V. L.; Luksch, P. *Acta Crystallogr., Sect. B: Struct. Sci.* **2002**, *58*, 364−369.

(46) Saal, J. E.; Kirklin, S.; Aykol, M.; Meredig, B.; Wolverton, C. *JOM* **2013**, *65*, 1501−1509.

(47) Kresse, G.; Hafner, J. *Phys. Rev. B: Condens. Matter Mater. Phys.* **1993**, *47*, 558−561.

(48) Kresse, G.; Furthmüller, J. *Comput. Mater. Sci.* **1996**, *6*, 15−50.

(49) Kresse, G. *Phys. Rev. B: Condens. Matter Mater. Phys.* **1996**, *54*, 11169−11186.

(50) Blöchl, P. E. *Phys. Rev. B: Condens. Matter Mater. Phys.* **1994**, *50*, 17953−17979.

(51) Perdew, J. P.; Ernzerhof, M.; Burke, K. *J. Chem. Phys.* **1996**, *105*, 9982−9985.

(52) Peelaers, H.; Van de Walle, C. G. *J. Phys.: Condens. Matter* **2014**, *26*, 305502−305508.

(53) Harl, J.; Schimka, L.; Kresse, G. *Phys. Rev. B: Condens. Matter Mater. Phys.* **2010**, *81*, 115126−115143.

(54) Yao, Z.; Kim, S.; Li, Q.; Wu, J.; He, J.; Aykol, M.; Wolverton, C. *Chem. Mater.* **2017**, in press.

(55) Li, Q.; Yao, Z.; Wu, J.; Mitra, S.; Hao, S.; Sahu, T. S.; Li, Y.; Wolverton, C.; Dravid, V. P. *Nano Energy* **2017**, *38*, 342−349.

(56) Chang, D.; Chen, M.-H.; Van der Ven, A. *Chem. Mater.* **2015**, *27*, 7593−7600.

(57) Yu, H.-C.; Ling, C.; Bhattacharya, J.; Thomas, J. C.; Thornton, K.; Van der Ven, A. *Energy Environ. Sci.* **2014**, *7*, 1760−1768.

(58) Michel, K. J.; Ozoliņš, V. *J. Phys. Chem. C* **2011**, *115*, 21443−21453.

(59) Michel, K. J.; Zhang, Y.; Wolverton, C. *J. Phys. Chem. C* **2013**, *117*, 19295−19301.

(60) Michel, K. J.; Wolverton, C. *Comput. Phys. Commun.* **2014**, *185*, 1389−1393.

(61) Hart, G.; Forcade, R. *Phys. Rev. B: Condens. Matter Mater. Phys.* **2008**, *77*, 224115−224126.

(62) Hart, G. L. W.; Forcade, R. W. *Phys. Rev. B: Condens. Matter Mater. Phys.* **2009**, *80*, 014120−014127.

(63) Hart, G. L. W.; Nelson, L. J.; Forcade, R. W. *Comput. Mater. Sci.* **2012**, *59*, 101−107.